Isotopic and modeling investigation of long-term protein turnover in rat tissues

Nathalie Poupin, Jean-François Huneau, François Mariotti, Daniel D. Tomé, Cecile C. Bos, Hélène Fouillet

Am J Physiol Regul Integr Comp Physiol 304: R218–R231, 2013.
First published November 7, 2012; doi:10.1152/ajpregu.00310.2012.

Isotopic and modeling investigation of long-term protein turnover in rat tissues

Nathalie Poupin,[1,2] Jean-François Huneau,[1,2] François Mariotti,[1,2] Daniel Tomé,[1,2] Cécile Bos,[1,2] and Hélène Fouillet[1,2]

[1]*INRA (Institut National de la Recherche Agronomique), CRNH-IdF (Centre de Recherche en Nutrition Humaine d'Ile de France), UMR914 Nutrition Physiology and Ingestive Behavior, Paris, France; and* [2]*AgroParisTech, CRNH-IdF, UMR914 Nutrition Physiology and Ingestive Behavior, Paris, France*

Submitted 9 July 2012; accepted in final form 6 November 2012

Poupin N, Huneau J, Mariotti F, Tomé D, Bos C, Fouillet H. Isotopic and modeling investigation of long-term protein turnover in rat tissues. *Am J Physiol Regul Integr Comp Physiol* 304: R218–R231, 2013. First published November 7, 2012; doi:10.1152/ajpregu.00310.2012.—Fractional synthesis rates (FSR) of tissue proteins (P) are usually measured using labeled amino acid (AA) tracer methods over short periods of time under acute, particular conditions. By combining the long-term and non-steady-state ^{15}N labeling of AA and P tissue fractions with compartmental modeling, we have developed a new isotopic approach to investigate the degree of compartmentation of P turnover in tissues and to estimate long-term FSR values under sustained and averaged nutritional and physiological conditions. We measured the rise-to-plateau kinetics of nitrogen isotopic enrichments ($\delta^{15}N$) in the AA and P fractions of various tissues in rats for 2 mo following a slight increase in diet $\delta^{15}N$. Using these $\delta^{15}N$ kinetics and a numerical method based on a two-compartment model, we determined reliable FSR estimates for tissues in which P turnover is adequately represented by such a simple precursor-product model. This was the case for kidney, liver, plasma, and muscle, where FSR estimates were 103, 101, 58, and 11%/day, respectively. Conversely, we identified tissues, namely, skin and small intestine, where P turnover proved to be too complex to be represented by a simple two-compartment model, evidencing the higher level of subcompartmentation of the P and/or AA metabolism in these tissues. The present results support the value of this new approach in gaining cognitive and practical insights into tissue P turnover and propose new and integrated FSR values over all individual precursor AA and all diurnal variations in P kinetics.

protein kinetics; compartmental modeling; fractional synthesis rate; nitrogen stable isotopes; isotope incorporation rate

THE BODY IS MADE UP OF NUMEROUS proteins (P) that differ markedly in their nature, function, and turnover kinetics. The different P of plasma and tissues are continuously synthesized from and degraded to free amino acids (AA), with synthesis and degradation rates that vary largely among P and as a function of nutritional, physiological, and pathophysiological conditions (52). This continuous turnover of P ensures their renewal with a relative flexibility in adapting to the environmental and endogenous variations. To understand how P homeostasis is achieved and controlled in health and disease, methods are needed to assess the rates of P turnover in tissues and to better understand its metabolic compartmentation. Much effort has been devoted to measuring the P synthesis rates, and several approaches have been proposed (12, 19, 20, 41, 52, 53), whereas little is known about P turnover compartmentation (1, 27, 28, 35, 52).

P fractional synthesis rates (FSR) in tissues and plasma are classically determined using precursor-product tracer methods, which consist in quantifying the temporal rate of incorporation into the studied P pool of an isotopically labeled AA tracer. The AA tracer is generally administered intravenously via a flooding dose or a constant infusion, so as to maintain a steady-state labeling of the AA precursor pool for P synthesis during a short measurement period of a few minutes or a few hours, depending on the infusion mode (12, 19, 20, 53), during which the tracer recycling from P breakdown can be neglected. However, these classic tracer methods have some limitations. In particular, their FSR estimates may be biased because of nonphysiological conditions that artificially increase the P turnover when the flooding-dose method is used and because of the large uncertainty regarding the isotopic enrichment of the true precursor pool when the constant-infusion method is used (12, 20). The FSR values reported in the literature, therefore, differ markedly, depending on the tracer method, the particular AA tracer, and the surrogate precursor pool for P synthesis that are used (20, 26, 49, 52).

Precursor-product AA tracer studies have established that the different body P have distinct FSR [e.g., much more rapid in gut and liver than in muscle (10, 52)] that are also differently stimulated by particular nutritional, physiological, and pathophysiological conditions (9, 19, 36, 52). Because of the necessarily limited duration of such AA tracer studies, most FSR modulations have been measured acutely over short time periods and have been reported to differ according to the particular metabolic state of the individual (i.e., fed or fasted), but it is difficult to extrapolate conclusions from such results regarding average FSR values over longer periods of time. Interestingly, the more recent and less familiar method of ^2H_2O administration makes it possible to obtain such long-term FSR estimates, because of the rapid equilibration between H labeling in body water and intracellular AA, which can therefore be kept at an isotopic steady state for long durations (21).

These existing precursor-product tracer methods are deliberately limited to the conditions of an isotopic steady state regarding the labeling of the pool that is assumed to be the precursor pool for P synthesis, because they are not designed to examine the degree of metabolic compartmentation of P turnover but share the common objective of relatively simply providing FSR estimates to facilitate their routine use in human studies. As a result, some of these FSR estimates may be biased, because they rely on simplifying assumptions relative to the structure and functioning of P turnover, which might be

Address for reprint requests and other correspondence: H. Fouillet UMR914 PNCA, AgroParisTech, 16 rue Claude Bernard, 75005 Paris, France (e-mail: Helene.Fouillet@agroparistech.fr).

erroneous, particularly in tissues that can involve metabolic or kinetic compartmentation that is more complex than generally assumed (27, 41, 52). As a consequence, despite the vast number of dedicated tracer studies in the literature, no consensus has been reached concerning the "true" FSR values of different P and, more problematically, how they are affected by different nutritional and pathophysiological conditions (19, 20, 41). This warrants the development of a new complementary approach that will enable the analysis of precursor-product relationships structurally (to identify and compare the degree of P turnover compartmentation in tissues) and kinetically (to determine long-term FSR values that integrate the numerous diurnal variations in P kinetics under sustained nutritional or physiological conditions).

For this purpose, we measured the kinetics of nitrogen isotopic enrichments (δ^{15}N) in the AA and P fractions of various rat tissues over a 2-mo period following a slight increase in the δ^{15}N of the diet. By comparing these postshift, rise-to-plateau δ^{15}N kinetics in AA and P under non-steady-state isotopic conditions for the precursor and the product, we investigated the compartmental structure of tissue P metabolism. Using a simple precursor-product model as the representation of tissue P metabolism, we developed a numerical method to estimate the averaged tissue P FSR values over the 2-mo experimental period. We also evidenced that some tissues display a P metabolism that is too compartmented to be described using a simple precursor-product model.

MATERIALS AND METHODS

Collection of Experimental Data

Animals and diets. Male Wistar rats (n = 43; Harlan, Gannat, France) were housed in a temperature-regulated (22 ± 2°C) room under a 12:12-h light-dark cycle (dark period from 0900 to 2100). Experiments were carried out in accordance with the recommendations of the National Institutes of Health *Guide for the Care and Use of Laboratory Animals*. The protocol was approved by the Ethics Committee for Animal Experiments (COMETHEA) of the Jouy-en-Josas Institut National de la Recherche Agronomique Centre and AgroParisTech (approval no. 11/009).

The rats were first maintained under standard conditions for a 5-wk equilibration period, with free access to a diet composed of 20% milk P, 30% lipids, and 50% carbohydrates and with a δ^{15}N of 4.9‰. At the end of this 5-wk equilibration period (referred to as *day 0* of the diet-shift experiment), the rats, weighing 343 ± 13 g, were switched for 2 mo to the same diet that had been slightly ^{15}N-enriched by the addition of ^{15}N-enriched milk P obtained as previously described (22). ^{15}N-enriched milk P accounted for 4.5% of the total quantity of P in the final diet, leading to a slightly ^{15}N-enriched diet with a δ^{15}N of 27‰ and the same nutrient composition as the initial diet. Rats were allowed free access to food from 0900 to 1900 (during the dark period) and had free access to water throughout the day. Body weight was measured twice weekly.

Experimental protocol and sampling procedures. Different groups of rats were killed on *day 0* (i.e., before the diet shift) and on *days 1, 2, 4, 8, 17, 31*, and *58* following the diet shift, with 5 rats in all groups except in the last group, which consisted of 8 rats. All the rats were euthanized after an overnight fast. The rats were anesthetized by inhalation of isoflurane. While the rats were under deep anesthesia, the abdomen was opened and a ~5-ml blood sample was quickly withdrawn from the vena cava. The animals were then killed by rupture of the aorta. The liver, small intestine, kidneys, and tibialis anterior muscle were rapidly dissected out, rinsed, weighed, and snap-frozen in liquid nitrogen. A sample of skin was also collected, and the skin was dissected out and weighed. The "stripped" carcass was prepared as follows: other abdominal and thoracic organs were discarded, and the distal parts of the limbs, head, and tail were severed. The stripped carcass was then weighed. All samples were stored at −20°C until analysis.

Sample preparation. In each sampled tissue, the P and non-P (AA) fractions were isolated. Frozen tissues were pulverized with a mortar and pestle cooled in liquid nitrogen and precipitated by addition of 700 μl of 5-sulfosalicylic acid (10%) per 100 mg of tissue. After centrifugation (2,500 *g*, 4°C, 15 min), the pellet was rinsed twice with 700 μl of 5-sulfosalicylic acid (10%), and the supernatant was extracted and filtered through 3-kDa cut-off filters (Amicon Ultra-4, Ultracel 3k, Millipore, Carrigtwohill, Ireland) to isolate the AA fraction. The soluble fraction (i.e., the non-P fraction containing the free AA) and the insoluble fraction (i.e., the P fraction containing the P-bound AA) were then freeze-dried.

In plasma, the different nitrogen fractions (P, AA, and urea) were also separated. The P fraction was isolated by precipitation with 200 μl of sulfosalicylic acid (1 g/ml). After 1 h of storage at 4°C and centrifugation (2,000 *g*, 4°C, 20 min), the pellet was rinsed with 1 ml of sulfosalicylic acid (1 g/ml), centrifuged again, and freeze-dried. The supernatant, containing AA and urea, was filtered through 3-kDa cut-off filters (Amicon Ultra-4) to eliminate residual P and large peptides. The filtrate was then buffered at pH 7 and transferred onto 0.2 ml of cation-exchange resin in the Na^+ form (Dowex AG50X8, Bio-Rad, Marnes-la-Coquette, France) in the presence of 10 μl of urease (Sigma) for 2 h at 30°C to bind the ammonium released from urea hydrolysis. The urea-depleted supernatant was acidified and transferred onto 0.2 ml of cation-exchange resin in the H^+ form (Dowex AG50X8, Bio-Rad) to bind the protonated AA. The resin containing the AA was washed with distilled water and dried in an oven at 50°C.

Elemental analysis and isotopic determinations. In each of the P and AA fractions isolated from tissues and plasma, the stable isotope ratios of nitrogen were determined using an isotope-ratio mass spectrometer (Isoprime, VG Instruments, Manchester, UK) coupled to an elemental analyzer (model EA 3000, EuroVector, Milan, Italy). Internal standards (tyrosine) were included in every run to correct for possible variations in the raw values measured by the mass spectrometer. Typical replicate measurement errors for these reference materials were ±0.2‰. Results were expressed using the delta notation according to the following equation

$$\delta^{15}N = [R_{sample}/R_{standard}) - 1] \times 1,000$$

where R_{sample} and $R_{standard}$ are the nitrogen isotope ratio of the heavier isotope to the lighter isotope (^{15}N/^{14}N) for the sample being analyzed and the internationally defined standard (atmospheric N_2, $R_{standard}$ = 0.0036765), respectively, and δ is the delta notation in parts per 1,000 (‰) relative to the standard.

The nitrogen percentage in each P and AA fraction of the samples was determined using the elemental analyzer (model EA 3000, EuroVector), with atropine as standard. Tissue samples were weighed before and after they were freeze-dried to estimate the tissue dry matter percentage, and the total nitrogen content (N) of each sampled tissue fraction was calculated using the following equation

$$N(mmol) = 1,000 \times (m \times \%DM/100 \times \%N/100)/14$$

where %N and %DM are the nitrogen and dry matter percentages measured in the sample, respectively, and m (g) is the total mass of the tissue. Total muscle mass was approximated by the stripped carcass mass. The nitrogen content of plasma P and AA fractions was calculated as the product of the nitrogen concentration in the fraction and the plasma volume, which was estimated as 2.91% × BM + 2.54, where BM is body mass (5).

Statistics. At *day 0*, differences in δ^{15}N between the P and AA fractions for each tissue were tested using *t*-tests. Differences between tissues were assessed using ANOVA followed by post hoc tests with

Tukey's adjustments for multiple comparisons between tissues. The effect of time on the total nitrogen content of each tissue fraction was determined by ANOVA (Proc GLM, SAS 9.1, SAS Institute, Cary, NC). $P \leq 0.05$ was considered significant.

FSR Estimation Using a Two-Compartment Model of P Turnover in Tissues

We tested the ability to infer the FSR value of a given tissue or plasma from the combined analysis of ^{15}N enrichments in its P and AA fractions after a shift in the ^{15}N enrichment of the diet (referred to as "diet shift"). We developed a compartmental, mechanistic model describing the δ^{15}N postshift kinetics in the P and AA fractions of a given tissue in relation to its FSR, together with a method for numerical identification of the FSR based on the model equations. This modeling approach relies on the following assumptions: *1*) P turnover in the studied tissue can be adequately described by a two-compartment model, with a precursor-product structure as described below, and *2*) the tissue is in an elemental steady state during the entire diet-shift period, i.e., its growth rate is null or negligible compared with its turnover rate. The numerical method for FSR estimation was first validated by verification of its ability to provide reliable FSR estimates when theoretical δ^{15}N postshift kinetics data simulated using known FSR values for a tissue P turnover system fulfilling the above assumptions were analyzed. The method was then applied to the real experimental data measured in each tissue. Fulfillment of the steady-state assumption was verified a priori on the basis of the measured nitrogen contents of tissues, whereas the assumption relative to the system structure was validated a posteriori when the numerical approach succeeded in identifying a FSR value for the tissue.

Model structure and equations. We developed a physiologically based two-compartment model describing the δ^{15}N kinetics in the AA and P nitrogen fractions of a given tissue after a change in the diet δ^{15}N in relation to its FSR. This model (Fig. 1) is made up of a precursor pool, which represents the free AA used for the P synthesis, and a product pool, which represents the tissue P. The nitrogen exchange fluxes between these two compartments depict the nitrogen exchanges that occur during the processes of P synthesis and breakdown. By considering a single P compartment, the FSR represents the weighted average of the different tissue P turnover rates. The assumption of elemental steady state for tissue AA and P fractions implies that the amounts of total nitrogen in the compartments and the total nitrogen fluxes are constant and that only the specific ^{15}N abundance in the P and AA pools is modified following the diet shift.

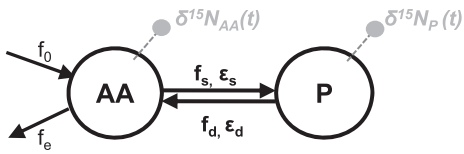

$$\mathrm{FSR} = f_s/N_P = \frac{\delta^{15}N_P(t+\Delta t) - \delta^{15}N_P(t)}{\int_t^{t+\Delta t}\delta^{15}N_{AA}(t)dt - \int_t^{t+\Delta t}\delta^{15}N_P(t)dt - (\varepsilon_s - \varepsilon_d)\cdot\Delta t}$$

Fig. 1. Two-compartment model of tissue protein metabolism. Circles indicate compartments, which represent free amino acids (AA) and proteins (P) in the tissue. Dashed lines with bullets indicate experimental measurements of nitrogen isotopic enrichments (δ^{15}N) in each compartment ($\delta^{15}N_{AA}$ and $\delta^{15}N_P$) at different times. Arrows represent nitrogen transfers between compartments: f_s and f_d are instantaneous fluxes of nitrogen transfer through P synthesis and breakdown, respectively, and f_0 and f_e are instantaneous fluxes of nitrogen transfer into AA from and toward outside the tissue, respectively. ε_s and ε_d represent isotope effects associated with P synthesis and P breakdown, respectively. Equation defining P fractional synthesis rate (FSR) is derived under the assumption that instantaneous total nitrogen fluxes and amounts of total nitrogen in the 2 compartments remain constant (see APPENDIX for complete derivation of the equation).

With use of this two-compartment model and in accordance with the mass conservation principle, the evolutions of the nitrogen isotopic enrichments of the P ($\delta^{15}N_P$) and AA ($\delta^{15}N_{AA}$) compartments following the diet shift were described by the following non-steady-state linear differential equations (see details for derivation of the equations in the APPENDIX)

$$d(\delta^{15}N_{AA})/dt = \left[\delta^{15}N_0(t) - \delta^{15}N_{AA}(t) - \varepsilon_e\right]\times\frac{f_0}{N_{AA}} + \left[\delta^{15}N_P(t) - \delta^{15}N_{AA}(t) + \varepsilon_d - \varepsilon_s\right]\times \mathrm{FSR}\times\frac{N_p}{N_{AA}} \quad (1)$$

$$d(\delta^{15}N_P)/dt = \mathrm{FSR}\times\left[\delta^{15}N_{AA}(t) - \delta^{15}N_P(t) + \varepsilon_s - \varepsilon_d\right] \quad (2)$$

where FSR is also equal to the P degradation rate under the steady-state assumption for total nitrogen, f_0 represents the flux of total nitrogen from plasma to the AA pool, $\delta^{15}N_0$ is the isotopic enrichment of the f_0 flux, N_{AA} and N_P are the amounts of total nitrogen in the AA and P pools, respectively, and ε_s, ε_d, and ε_e represent the isotope effects associated with P synthesis, P breakdown, and AA exportation from the AA pool to plasma, respectively. These isotopic effects account for the potential isotope fractionation associated with these metabolic reactions and are defined as the difference between the isotopic enrichment of the instantaneous flux and that of the pool from which it arises. It should be noted that the difference between ε_s and ε_d represents the difference between $\delta^{15}N_P$ and $\delta^{15}N_{AA}$ at isotopic equilibrium.

Numerical approach for FSR estimation and practical implementation. From the $\delta^{15}N_P$ and $\delta^{15}N_{AA}$ data sampled at different time points, FSR values can be calculated using *Eq. 2*. To numerically identify the FSR values, we adopted the approach described as follows.

By integrating *Eq. 2*, one can express the change in δ^{15}N in the P compartment over a time interval Δt as

$$\Delta\delta^{15}N_P(t) = \mathrm{FSR}\times\left[\int_t^{t+\Delta t}\delta^{15}N_A(t)\cdot dt - \int_t^{t+\Delta t}\delta^{15}N_P(t)\cdot dt\right] + \mathrm{FSR}\times\Delta\varepsilon\times\Delta t \quad (3)$$

where $\Delta\delta^{15}N_p(t) = \delta^{15}N_p(t+\Delta t) - \delta^{15}N_p(t)$ and $\Delta\varepsilon = (\varepsilon_s - \varepsilon_d)$.

Equation 3 was preferred to *Eq. 2*, because calculating the derivative of a given curve from discrete and noisy data generally produces a more important relative error than calculating its area under the curve. In addition, to minimize the error on the calculated integrals for $\delta^{15}N_A$ and $\delta^{15}N_P$, we modeled each of the kinetics for $\delta^{15}N_A$ and $\delta^{15}N_P$ by a sum of two exponential functions. The parameters of these functions were identified by fitting the equations to the experimental $\delta^{15}N_A$ and $\delta^{15}N_P$ data using the nonlinear least-squares method of the curve-fitting toolbox (version 1.1.7) in MATLAB (version 7.7, MathWorks, Natick, MA). The fitted equations were subsequently used to calculate $\Delta\delta^{15}N_P$ values and $\delta^{15}N_A$ and $\delta^{15}N_P$ integrals over any chosen Δt interval during the subsequent procedure for the numerical resolution of *Eq. 3*, which is described below.

The two unknown parameters in *Eq. 3*, FSR and $\Delta\varepsilon$, can be determined by solving a system of n linear equations, composed of *Eq. 3* applied to n different time intervals of length Δt, with $n \geq 2$ (so as to have more equations than unknowns). Time intervals Δt were chosen as subintervals of the experimental period. For a set of n intervals, the system of n equations was solved as a nonlinear least-squares minimization problem, by searching for the minimum of function F

$$F = \sum_{i=1}^{n}(F_i^2)$$

where $F_i = \mathrm{FSR}\times[\int_{t_i}^{t_i+\Delta t}\delta^{15}N_A(t) - \int_{t_i}^{t_i+\Delta t}\delta^{15}N_P(t)] + \mathrm{FSR}\times\Delta\varepsilon\times\Delta t - [\delta P(t_i+\Delta t) - \delta P(t_i)]$. The solution was achieved by using a trust-region algorithm under MATLAB (lsqnonlin function) and yielded one FSR estimate for each set of n intervals.

To test whether numerical FSR estimates depend on the number n and length Δt of the time intervals chosen, we tested different options for n and Δt. By varying n and Δt, we divided the whole 0- to 60-day experimental period into different intervals of equal length, or we randomly selected time intervals of various length within the whole period in such a way that they did not overlap and first completely and then incompletely covered the experimental period. Because all the partitioning methods thus tested produced comparable results, we finally used the simplest approach: we divided the whole period into n intervals of equal length Δt ($\Delta t = 60/n$ days), with Δt being a whole number of days (i.e., with Δt = 30, 20, 15, 12, 10, 6, 5, 4, 3, 2, or 1 days, when n = 2, 3, 4, 5, 6, 10, 12, 15, 20, 30, or 60 intervals, respectively). For each partition into n intervals of Δt, solving the system of n equations produced one FSR estimate. Since the different FSR estimates varied very little among the different partitions tested (except those obtained in the 2 extreme cases with n = 2 and 60), we retained as the final FSR estimate the average of the different estimates obtained from all tested partitions with n = 3–30 intervals.

Evaluation of the validity of the method. To estimate the reliability of the FSR estimates generated using this method, it was tested on theoretical data for $\delta^{15}N_A$ and $\delta^{15}N_P$ postshift kinetics simulated from known parameter values. Two distinct and adequate sets of parameters (FSR and $\Delta\varepsilon$) were chosen and assigned to the two-compartment model to generate two distinct profiles for $\delta^{15}N_A$ and $\delta^{15}N_P$ kinetics: a fast-FSR profile and a slow-FSR profile, which were simulated using FSR values corresponding to the mean FSR values reported in rat studies for liver (70%/day) and muscle (15%/day), respectively. For each profile, the simulated $\delta^{15}N_A$ and $\delta^{15}N_P$ data were generated at each of the eight experimental sampling time points with or without addition of a normally distributed random noise (with a standard deviation of 0.1), intended to mimic the experimental error and interindividual variability as observed in our data set. One hundred different sets of noisy data were generated for each profile, and the FSR parameter was then estimated from the noise-free data and from each set of noisy data using the numerical approach described above (i.e., fitting of the data with sums of exponential functions, partitioning the whole period into various n numbers of intervals of equal length, and estimating the FSR as the average of the estimated values for all possible partitions of the period into n intervals, except with n = 2 or 60 intervals). In each case, the FSR estimate was compared with the a priori value used to generate the data sets to evaluate the accuracy and precision of the method.

Sensitivity analysis and test of the method over shorter experimental periods. A sensitivity analysis was performed to study the influence of the FSR parameter on the behavior of the system and, more particularly, to identify the time periods when the FSR value had the strongest impact on the postshift $\delta^{15}N$ kinetics in the AA and P pools. This was done for the fast- and slow-FSR theoretical profiles by simulating the changes in $\delta^{15}N_A$ and $\delta^{15}N_P$ in response to 10% and 25% increases and decreases in the FSR value.

To determine whether the duration of the experimental period impacted the accuracy and precision of FSR estimates, we tested the method developed when considering experimental periods shorter than our entire 2-mo period. FSR values were reestimated from the set of simulated noisy data (for slow- and fast-FSR profiles) using successively only the first five data points (i.e., corresponding to a restricted duration of ~1 wk) and then the first 6 data points (i.e., corresponding to a restricted duration of ~2 wk). FSR estimations over these shortened time periods were performed as described above.

Test of Alternative Model Structures for Some Specific Tissues

The developed method was applied to the experimental data sets for $\delta^{15}N_A$ and $\delta^{15}N_P$ measured in each tissue and plasma. In tissues for which we were unable to identify numerical values for FSR, we concluded that the hypothesized precursor-product model was too simple to accurately fit the experimental data, and we tested whether models with a more complex structure could conversely account for the $\delta^{15}N_A$ and $\delta^{15}N_P$ kinetics observed in these tissues. Models with additional AA or P pools were investigated: $\delta^{15}N_A$ and $\delta^{15}N_P$ were simulated from those models and compared with experimental data, and parameter optimization was performed on different model structures to determine numerical parameter values that would enable the model to generate the closest predictions to the observed $\delta^{15}N_A$ and $\delta^{15}N_P$ kinetics. We used the SimBiology toolbox (version 2.2) of MATLAB to implement the models and their equations and to simulate the evolutions of total nitrogen and isotope abundances in the different pools, while the parameter estimation was implemented under MATLAB.

RESULTS

Experimental Data

The experimental data for $\delta^{15}N$ postshift kinetics in the different AA and P fractions of tissues are reported in Fig. 2. At the beginning of the diet shift (*day 0*), $\delta^{15}N$ values in the different plasma and tissue fractions were generally higher than that of the diet, except in the AA fractions of muscle and plasma, where the $\delta^{15}N$ values were, respectively, lower than and similar to that of the diet. There were also significant $\delta^{15}N$ differences among tissues and between the two nitrogen fractions of a given tissue, with higher $\delta^{15}N$ values in the P fraction than in the AA fraction of all tissues.

After the diet shift, all the sampled AA and P fractions of plasma and tissues incorporated the new $\delta^{15}N$ of the diet following biexponential rise-to-plateau kinetics (Fig. 2). The incorporation rates differed markedly among tissues (e.g., with faster rates in liver and plasma than in muscle fractions) and also slightly between fractions within a given tissue (with slightly faster rates in the AA fraction than in the P fraction). The $\delta^{15}N$ postshift evolutions remained, however, virtually parallel between the AA and P fractions in all sampled tissues, except in skin, where the $\delta^{15}N$ evolution was markedly faster in the AA fraction than in the P fraction.

Contrary to the $\delta^{15}N$ values, the total nitrogen contents in the AA and P fractions of most of the sampled tissues did not change over time, except for an increase in the muscle P fraction and plasma AA and P fractions and a decrease in the small intestine AA and P fractions. However, these changes were moderate, with, for instance, an average increase of 0.4%/day in the nitrogen contents of the muscle and plasma P fractions over the experimental period, which is negligible compared with the reported FSR values for these tissues.

FSR Estimation Using the Two-Compartment Model

Sensitivity analysis of the system behavior and theoretical validity of the method of FSR estimation. The simulated $\delta^{15}N_A$ and $\delta^{15}N_P$ kinetics for the fast- and slow-FSR profiles (Fig. 3), which were used to conduct the sensitivity analysis and test the validity of our method of FSR estimation, satisfactorily resembled the evolutions of $\delta^{15}N_A$ and $\delta^{15}N_P$ measured in liver and muscle, respectively (Fig. 2, *A* and *B*). The sensitivity analysis indicated that a change in the FSR value exerted a different effect on $\delta^{15}N$ kinetics, depending on the FSR profile. With the fast-FSR profile, the impact of an FSR variation was significant at the early time points, and particularly during the first 2 wk after the diet shift, but was transient (Fig. 4, *A* and *B*), whereas this impact was slightly delayed but more sustained over the entire postshift period with the slow-FSR profile and, more

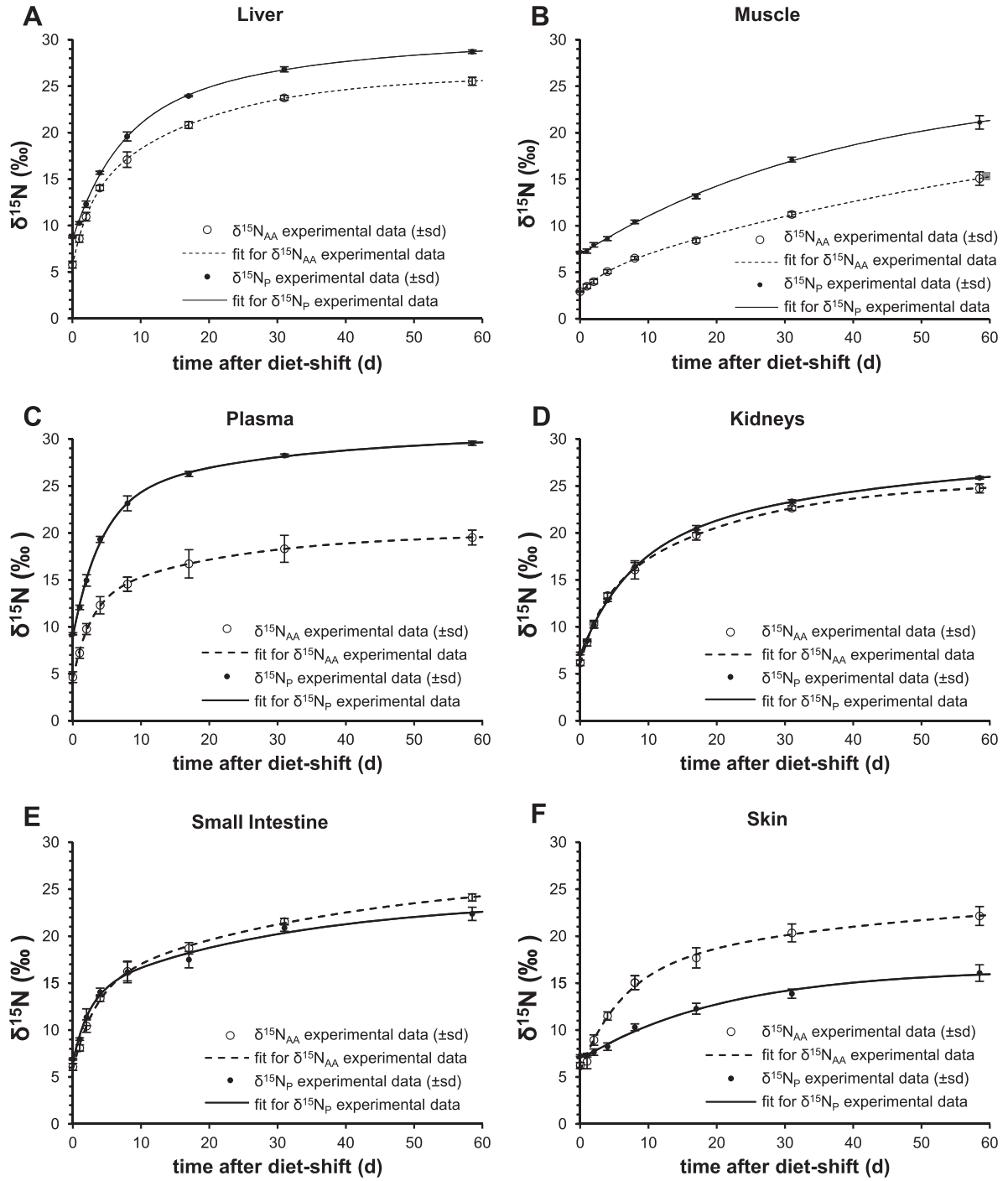

Fig. 2. Experimental $\delta^{15}N_{AA}$ and $\delta^{15}N_P$ kinetics measured in tissues after diet shift. Experimental data (○ and ●) are means ± SD of $\delta^{15}N_{AA}$ and $\delta^{15}N_P$, respectively ($n = 5$ for *sampling times 1–7* and $n = 8$ for *sampling time 8*) of liver (*A*), muscle (*B*), plasma (*C*), kidney (*D*), small intestine (*E*), and skin (*F*). Experimental $\delta^{15}N_{AA}$ and $\delta^{15}N_P$ data were fit to sums of 2 exponential functions (dashed and solid lines, respectively).

particularly, in the P fraction (Fig. 4, *D* and *E*). In addition, an increase (decrease) in the FSR value exerted a different impact on the $\delta^{15}N_P$ and $\delta^{15}N_{AA}$ kinetics, by increasing (lowering) $\delta^{15}N_P$ values while lowering (increasing) $\delta^{15}N_{AA}$ values. Consequently, the difference between $\delta^{15}N_P$ and $\delta^{15}N_{AA}$, which is a major determinant for FSR estimation (see *Eq. 3*), was positively sensitive to variations in FSR. This effect was more marked but also more transient with the fast-FSR profile, with an impact that was significant only during the first 2 wk, by comparison with the slow-FSR profile, where the effect was smaller but persisted for the entire 2-mo postshift period (Fig. 4, *C* and *F*). These results indicate that the early postshift period is the most informative with respect to FSR estimates in rapidly turning-over tissues, contrary to slowly turning-over tissues, where longer-term $\delta^{15}N$ kinetics remain informative regarding FSR values.

To test the validity of the method, we attempted to reestimate, from the noise-free and the noisy simulated data sets, the FSR

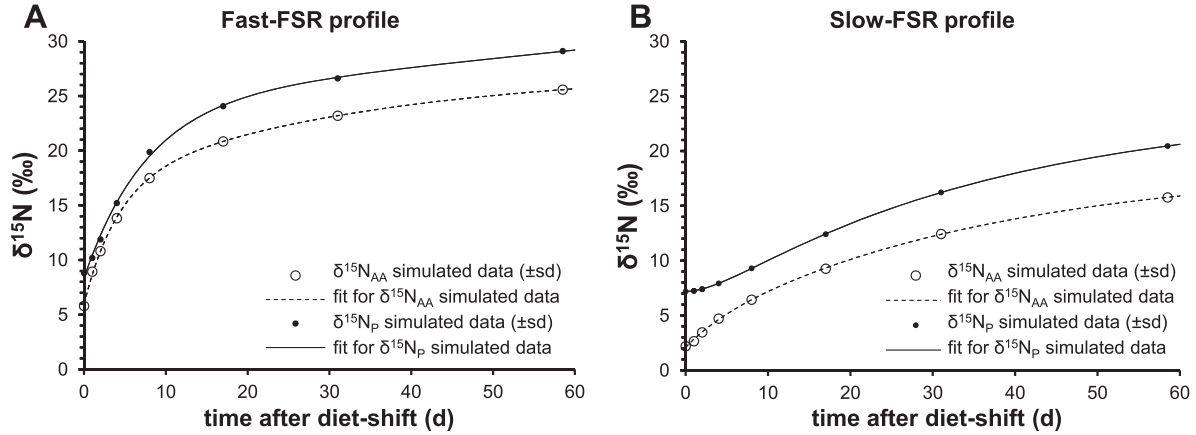

Fig. 3. $\delta^{15}N_{AA}$ and $\delta^{15}N_P$ postshift kinetics simulated from a 2-compartment model for tissues with fast or slow FSR. Theoretical $\delta^{15}N_{AA}$ and $\delta^{15}N_P$ kinetics with a fast-FSR profile (*A*) and a slow-FSR profile (*B*) were simulated at each sampling time using the 2-compartment model, with FSR values of 15 and 70%/day, respectively. Simulated data were fit to sums of 2 exponential functions (dashed and solid lines, respectively).

value used to generate those data. The FSR estimates and comparisons with the known true values are reported in Table 1. FSR values were estimated with a very good accuracy from the noise-free and noisy simulated data sets for both profiles, with a percent difference from known values (i.e., %error) of ~4% for the fast-FSR profile and 6% for the slow-FSR profile. The method also estimated FSR values with a very good precision (as shown by the small coefficients of variation of 7.5% and 12.5% for the fast- and slow-FSR profiles, respectively, when tested using the noisy simulated data sets).

Having identified the first 2 wk after the diet shift as the time period when $\delta^{15}N_A$ and $\delta^{15}N_P$ kinetics were most markedly impacted by the FSR value, we reestimated the FSR over experimental time periods <2 mo (Fig. 5). For both profiles, the accuracy of FSR estimates was slightly improved when the sampling scheme was restricted to the first 2 wk [with an error of 2% (instead of 4%) and 4% (instead of 6%) for the fast- and slow-FSR profiles, respectively], while it was slightly impaired when the sampling scheme was limited to only 1 wk (with errors of 10% and 7% for the fast- and slow-FSR profiles, respectively). The precision of the FSR estimates was significantly impaired when the time period was shortened from 2 mo to 2 wk and 1 wk, with coefficients of variation that progressively rose from 7.5% to 10.6% and 21.7% for the fast-FSR profile and from 12.4% to 29.0% and 34.5% for the slow-FSR profile. These results show that, from a theoretical standpoint, the FSR in rapidly turning-over tissues can still be estimated with very good accuracy and precision when the experimental duration is limited to 2 wk, while for slowly turning-over tissues, this restriction does not affect the accuracy but impairs the precision of the estimates.

Numerical estimation of FSR in tissues from experimental data. Using the method thus developed, we were able to identify numerically FSR values from the experimental data obtained in liver, muscle, kidney, and plasma (Table 2). When taking into account the data measured over the whole 2-mo experimental period, we estimated FSR values of 103%/day in kidney, 101%/day in liver, 58%/day in plasma, and 11%/day in muscle. When this numerical estimation was performed using the data obtained only during the first 2 wk, we obtained new FSR estimates that were very close to those found previously for kidney (97%/day) and plasma (55%/day) but lower for liver (71%/day) and higher for muscle (18%/day).

Identification of the Degree of Compartmentation of P Metabolism for the Different Tissues

The fact that we were able to identify FSR values in liver, muscle, kidney, and plasma using the developed method indicates that the long-term processes of P breakdown and synthesis in such tissues are adequately described by the simple and standard precursor-product structure and dynamics assumed in our two-compartment model. By contrast, in the two other sampled tissues (small intestine and skin), our method generated null or negative values for FSR estimates or produced estimates that differed greatly, depending on the intervals chosen for the numerical resolution. As a result, we could not identify the model parameters from the experimental data sets obtained in these tissues, although our method was proven to be theoretically able to provide reliable FSR estimates from data sets simulated for a wide range of FSR values using our simple, precursor-product, two-compartment model. We concluded that this model is too simple to account for the variations in $\delta^{15}N_A$ and $\delta^{15}N_P$ in these tissues, likely because of the more complex compartmentation of the AA and P metabolism in such tissues.

To further investigate this point, we compared the ability of different models of increasing order to reproduce the $\delta^{15}N$ kinetic profiles observed in the AA and P fractions of skin and small intestine. In particular, we identified that the simplest models that adequately reproduced skin $\delta^{15}N$ kinetics were two different three-compartment models where the P fraction is represented by two distinct compartments, in a catenary or mammillary structure, with a nitrogen disappearance flux toward outside the system from one of them (Fig. 6). Using the SimBiology toolbox and a parameter optimization strategy under MATLAB for each of these three-compartment models, we found several distinct numerical parameterizations (i.e., values of transfer rates and discrimination coefficients) that produced satisfactory and similar fits between the model predictions and the $\delta^{15}N_A$ and $\delta^{15}N_P$ kinetics observed in skin (Fig. 6*C*). More specifically, for both models, various parameterizations, including FSR values between 15 and 25%/day, enabled very good and similar fits, but this FSR estimation was not reliable because of numerical identifiability problems. For such three-compartment models, we were also unable to

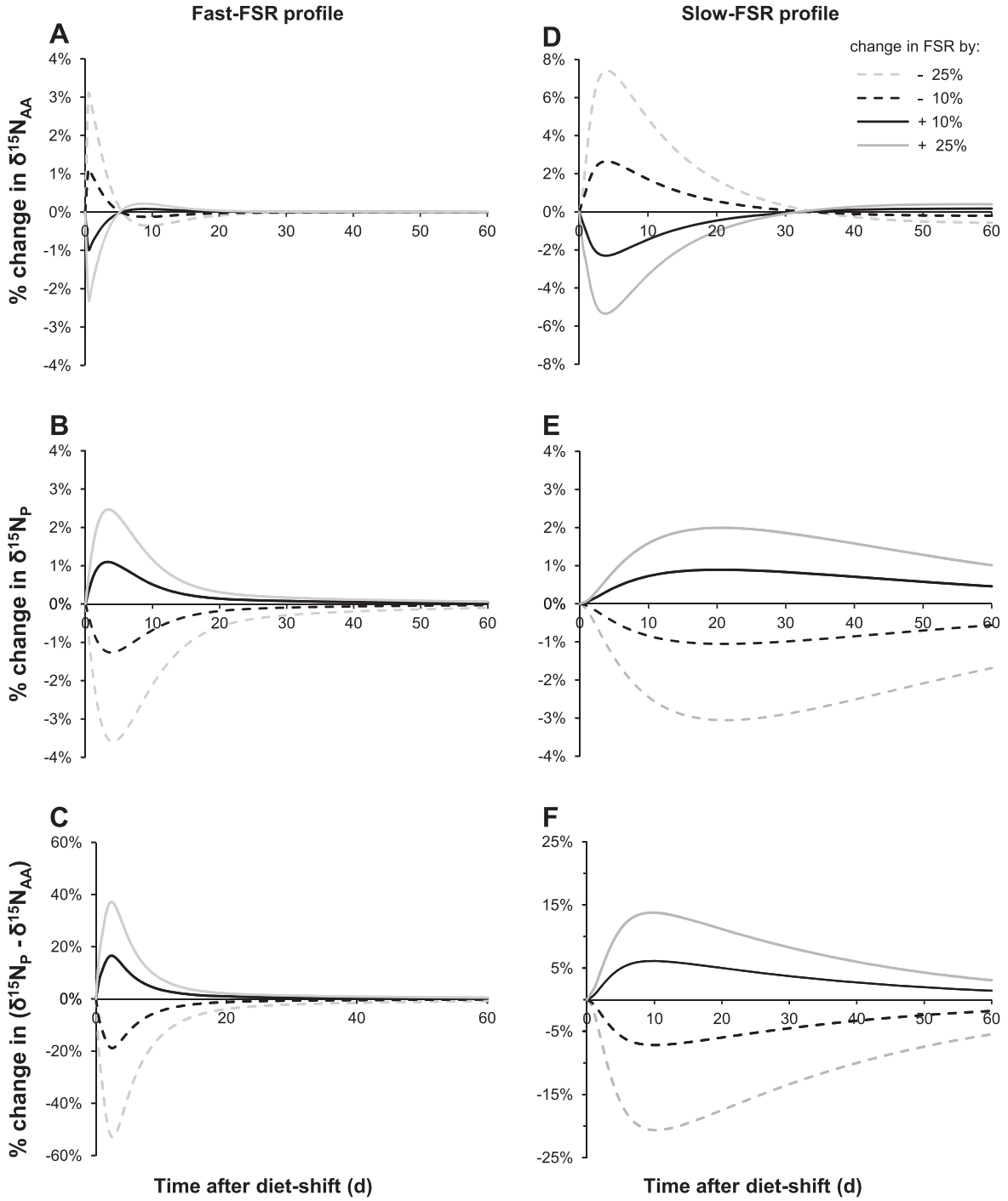

Fig. 4. Sensitivity of $\delta^{15}N_{AA}$ and $\delta^{15}N_P$ kinetics to variations in FSR. Curves are percent changes in simulated $\delta^{15}N_{AA}$ (*A* and *D*) and $\delta^{15}N_P$ (*B* and *E*) compartments and effect on the $\delta^{15}N_P$-$\delta^{15}N_{AA}$ variable (*C* and *F*) when FSR was decreased or increased by 10% or 25% for the fast-FSR (*left*) and slow-FSR (*right*) simulated profiles (i.e., with FSR varying from 70 to 52.5, 63.0, 77.0, and 87.5%/day for the fast-FSR profile and from 15 to 11.3, 13.5, 16.5, and 18.8%/day for the slow-FSR profile).

implement an analytical method for FSR identification similar to that developed for the two-compartment model because of the greater complexity of the differential equation describing evolution of $\delta^{15}N$ in the total P fraction.

DISCUSSION

We have developed a new method for the investigation of P turnover in rat tissues over long periods of time that produces global, integrated FSR values under sustained nutritional and physiological conditions. We demonstrated that a simple precursor-product model was sufficient to adequately describe P turnover under these averaged conditions in some tissues, such as liver and muscle, but was too simple and insufficient to reliably account for the complexity of P metabolism in other more compartmented tissues, such as small intestine and skin.

Table 1. *FSR estimates from simulated data and comparison with true known values*

	FSR, %/day				
		Estimates obtained from simulated data			
			With noise		
Profile Type	True values	Without noise	Value	CV, %	95% CI
Fast-FSR	70	67.1	67.2	7.5	57.3–77.0
Slow-FSR	15	14.1	14.1	12.4	10.7–17.5

Estimates are mean values obtained by averaging estimated fractional synthesis rate (FSR) from partitions of the whole time period into 3, 4, 5, 6, 10, 12, 15, 20, and 30 intervals. CV, coefficient of variation; CI, confidence interval.

Table 2. *FSR estimates from experimental data*

	FSR, %/day				
	Estimates from experimental data		Data from the literature		
Tissue	2-mo period	2-wk period	Mean ± SD	*n*	Range
Kidney	103	97	67 ± 21	16	29–93
Liver	101	71	83 ± 19	43	48–131
Plasma	58	55	47 ± 22	7	18–75
Muscle	11	18	9 ± 3	52	4–20

FSR estimates from experimental data over the entire 2-mo experimental period were obtained from the data at 8 sampling times: 0, 1, 2, 4, 8, 17, 31, and 58 days. FSR estimates from the experimental data over 2 wk were obtained from the data at the first 6 sampling times (0, 1, 2, 4, 8, and 17 days). FSR values from the literature were obtained from studies performed in adult rats using classic tracer methods (Refs. 2, 3, 7–11, 13–18, 23–25, 29, 32–34, 37, 39, 40, 42–44, 50).

Developed Method for FSR Estimation: Theoretical Validation and Application to Experimental Data

The method we developed relies on measurement of $\delta^{15}N$ kinetics in the AA and P fractions of tissues over a 2-mo period following a slight increase in the $\delta^{15}N$ of the diet and their numerical analysis using a simple two-compartment, precursor-product model for tissue P metabolism (Fig. 1). We validated this method theoretically by demonstrating its ability to provide FSR estimates with a good accuracy (<6% error) and precision (coefficient of variation <13%) from simulated $\delta^{15}N_P$ and $\delta^{15}N_{AA}$ kinetics (Table 1).

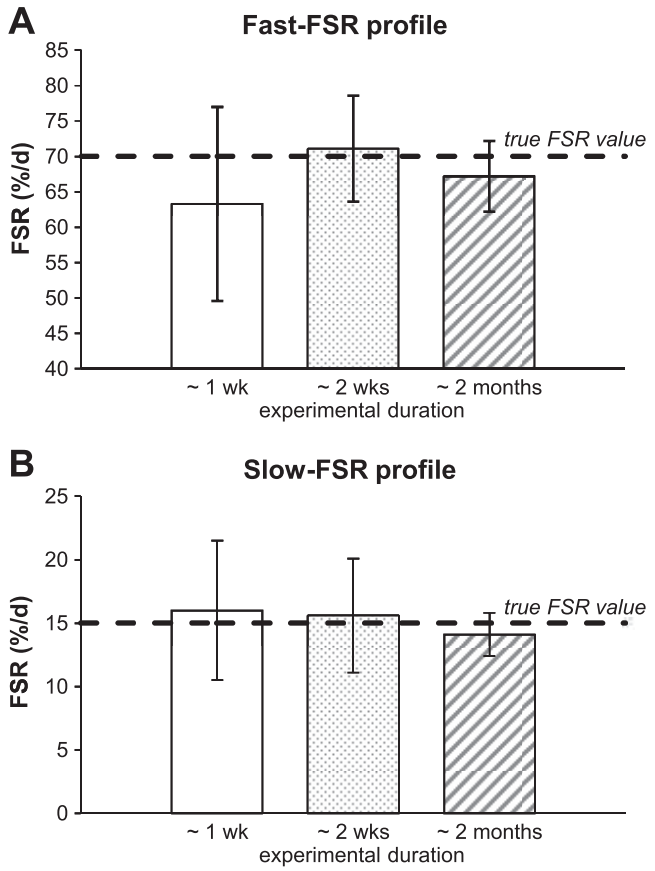

Fig. 5. FSR estimates obtained from noisy simulated data for fast-FSR (*A*) and slow-FSR (*B*) profiles, depending on duration of experimental period. Values are means ± SD of FSR estimates from 100 noisy data sets simulated for each FSR profile, with estimations performed over experimental durations of ~1 wk, ~2 wk, and ~2 mo [i.e., with all the sampling times (t = 0, 1, 2, 4, 8, 17, 31, and 58 days) for the ~2-mo duration, only the first 6 sampling times (corresponding to the 0- to 17-day period) for the ~2-wk duration, and the first 5 sampling times (corresponding to the 0- to 8-day period) for the ~1-wk duration].

When applied to real experimental data sets, the method yielded reliable FSR estimates in liver, muscle, kidney, and plasma. These FSR estimates were within the ranges of those previously reported in the literature using different classic AA tracer methods (i.e., AA flooding dose or continuous infusion) in well-fed, healthy rats of similar age for all tissues except kidney, where our estimates were slightly above the range of the values in the literature (Table 2). However, FSR values in the literature varied considerably, depending on the studies, by up to five- or threefold for muscle or kidney, respectively. Given the singularity of our approach compared with classic AA tracer studies and the fact that FSR estimations in such studies appear to be strongly dependent on the particular method and specific experimental conditions (20, 26, 49, 52), comparisons between our results and the literature should remain qualitative only and cannot be used as an external validation of our approach. However, the ranking of tissues according to their FSR values was globally the same when comparing the results of the present method and mean data in the literature (Table 2). By contrast, our FSR estimate for kidney was as high as that for liver, while it is, on average, lower in the literature. Nevertheless, the separate studies that have concomitantly examined FSR values in kidney and liver have reported contrasting results, with FSR values lower than (7, 10, 13, 23, 34), similar to (7, 10, 14, 15), or even higher than (32) those in kidney than liver.

Specificity of the Developed Method and Practical Adaptability to Other Experimental Conditions

The formula that we used for FSR estimation (Fig. 1) is actually closely related to the FSR formula that was used in classic AA tracer studies (51); the difference was that two supplemental terms are subtracted from the denominator in our formula. Inclusion of these two terms is necessary to avoid the two usual simplifications that are false in our context and refers to the specificity of our approach.

The first added term (i.e., the area under the curve of $\delta^{15}N_P$) accounts for the fact that, during the time period under consideration, part of the ^{15}N-enriched AA (i.e., arising from the

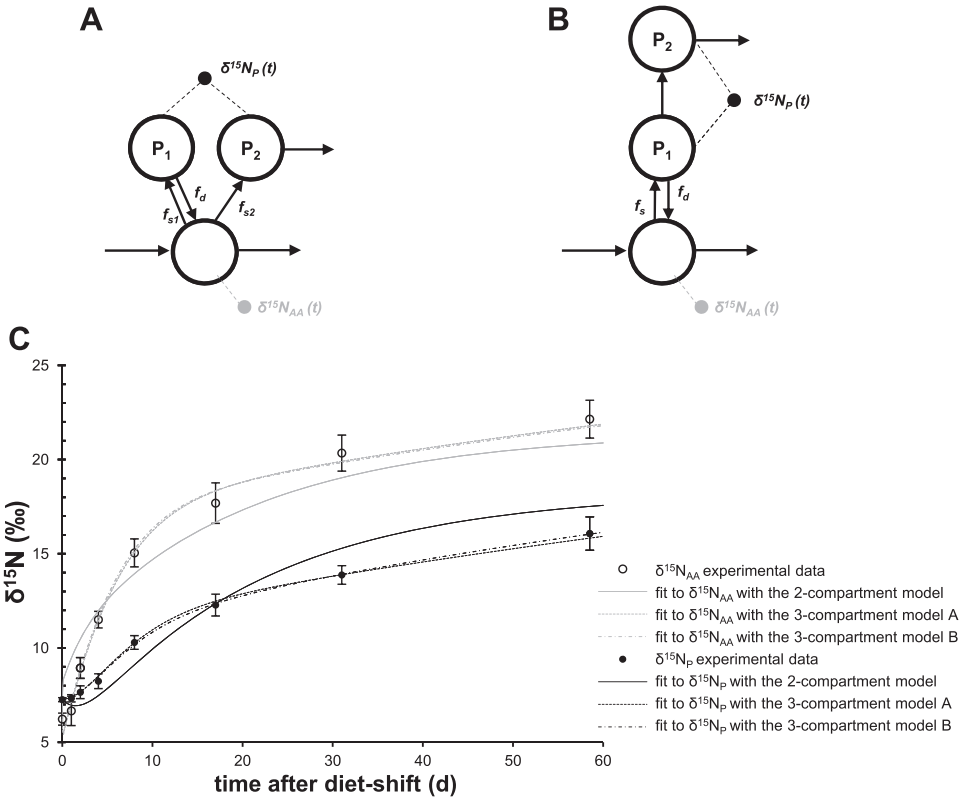

Fig. 6. Ability of different models to fit $\delta^{15}N_{AA}$ and $\delta^{15}N_P$ data in skin. Two 3-compartment candidate models [composed of 2 P compartments (P_1 and P_2) and 1 AA compartment (AA) in a mammillary (*A*) or a catenary (*B*) structure (*A* and *B*)] tested for their ability to better fit skin data than the 2-compartment model of Fig. 1. Dashed lines with bullets indicate experimental measurements of $\delta^{15}N_{AA}$ and $\delta^{15}N_P$, the nitrogen isotopic enrichments of the AA and P fractions of skin, respectively, with the P fraction being the sum of the P_1 and P_2 compartments. In *C*, solid, dashed, and dashed-dotted lines are model predictions obtained using the 2-compartment model, the 3-compartment model shown in *A*, and the 3-compartment model shown in *B*, respectively, that best fit the $\delta^{15}N_{AA}$ and $\delta^{15}N_P$ experimental data. $\delta^{15}N_{AA}$ (○) and $\delta^{15}N_P$ (●) experimental data are means ± SD.

^{15}N-enriched diet) that is incorporated into P is then lost from P by proteolysis, returning to the free AA compartment. This term related to tracer recycling is usually neglected in the short-term AA tracer studies, because the loss of labeling from the P compartment through proteolysis is quantitatively small during a short experimental duration of a few minutes to a few hours. This postulate becomes, however, more questionable in studies investigating the FSR of rapidly turning-over P and/or in studies involving a longer AA infusion (47, 53). In this regard, the almost parallel evolution of $\delta^{15}N$ in the AA and P fractions (as evidenced in the data obtained over our 2-mo investigation) shows that the continuous AA reutilization is considerable and not negligible in our context. Because the approach we developed accounts for recycling, it enables estimates over long time periods.

The second added term relates to the overall isotopic effect associated with P turnover (i.e., $\varepsilon_s - \varepsilon_d$; see the APPENDIX for definitions) and accounts for the natural difference in $\delta^{15}N$ between the P and AA fractions at the isotopic steady state. On *day 0* of the diet shift, we observed higher $\delta^{15}N$ values in the P fraction than in the AA fraction of all tissues, with absolute differences ranging from ~1‰ to 6‰. This is consistent with our previous report that, at natural abundance levels, $\delta^{15}N$ values are higher in the P fraction than in the AA fraction in most rat tissues (38). This difference in $\delta^{15}N$ between the P and AA fractions is linked to the existence of isotopic effects throughout one or several of the metabolic pathways within tissues, with a preferential utilization of AA containing the lighter (^{14}N), rather than the heavier (^{15}N), nitrogen isotope during metabolic interconversions of AA (30), P synthesis (45), and/or P breakdown (46). Inclusion of fractionation factors (i.e., ε_s and ε_d) in our mathematical representation appropriately accounts for these isotopic effects and their impact on the difference between $\delta^{15}N_P$ and $\delta^{15}N_{AA}$ at the isotopic equilibrium. In AA tracer studies, isotopic effects are neglected, because in this context the levels of AA enrichments are much higher than natural levels. By contrast, in our case, the term relative to the net isotopic effect (i.e., $\Delta\varepsilon = \varepsilon\varepsilon_s - \varepsilon_d$) was required and was not negligible compared with the other denominator terms, because our postshift diet was only slightly ^{15}N-enriched, so that postshift $\delta^{15}N_{AA}$ values remained of the same order of magnitude as $\Delta\varepsilon$.

Another specificity of our method is that it uses nitrogen, and not a specific AA, as the tracer, so that it provides mean FSR estimates for all individual AA in the precursor pool, whereas other methods produce FSR values that may vary according to the AA chosen as the tracer.

Our approach can be applied in the case of nongrowing tissues (i.e., elemental steady state) or in the presence of a significant P accretion and fractional rate of growth (FGR), by using the simplified *Eq. 3* or the nonsimplified *Eq. 4*, respectively, for FSR estimation (with *Eq. 4* including a supplemental positive term proportional to the FGR, i.e., $FGR \times \varepsilon_d \times \Delta t$; see the APPENDIX). In this study, the rats were in their late phase of growth during the 2-mo experimental period, and we used the simplified *Eq. 3*, because the nitrogen sizes of the plasma and tissue AA and P fractions were constant or displayed only a moderate increase, with a null or negligible FGR value relative to the FSR value in each tissue. Only plasma and muscle had nonnull FGR values, which were ~0.4%/day and, thus, negligible by comparison with their estimated FSR of 58 and 11%/day, respectively (the term $FGR \times \varepsilon_d \times \Delta t$ was 10–50 times smaller than the other terms of the equation for plasma and muscle, and we verified that it could be disregarded with

no effect on FSR estimates). However, by using the nonsimplified *Eq. 4*, our method could usefully be applied to any condition in which P synthesis differs from P degradation, such as the anabolic or catabolic conditions of net P accretion or loss, respectively (e.g., growth, exercise, malnutrition, sarcopenia, and diabetes). In such contexts, our method could be used to concomitantly estimate the FSR and fractional degradation rate (FDR) when measuring the FGR (since FDR = FSR − FGR). This would be particularly useful in nutrition and health studies investigating the ability of a given diet or treatment to modulate the balance between P synthesis and degradation.

Furthermore, under our long-term approach, the question of using a time window that is truly informative regarding FSR values was of particular importance. As detected from the sensitivity analysis performed on our simulated data, late $\delta^{15}N$ kinetics were less informative than early $\delta^{15}N$ kinetics with respect to FSR values, particularly in rapidly turning-over tissues. For the fast-FSR profile, the time point from which $\delta^{15}N$ kinetics were no longer informative regarding the FSR value (~2 wk; Fig. 4*C*) was nevertheless delayed compared with the time necessary to reach complete elemental turnover (~2 days, given the FSR value of 70%/day). This was because $\delta^{15}N_{AA}$ levels rose slowly and gradually after the diet shift, so that FSR durably impacted the coupled $\delta^{15}N_P$ and $\delta^{15}N_{AA}$ kinetics (and $\delta^{15}N_P - \delta^{15}N_{AA}$, which is a major determinant for FSR estimation; see *Eq. 3*), despite a rapid transfer to $\delta^{15}N_P$ of $\delta^{15}N_{AA}$ variations. Indeed, the dietary AA inflow that induced the $\delta^{15}N$ shift in tissues was small compared with the endogenous AA fluxes between and within tissues, which slowed the $\delta^{15}N_{AA}$ rise to plateau by continuously reintroducing ^{15}N enrichment levels lower than that of the diet, for as long as each body pool (even those with a slow turnover) had not reached its new isotopic steady state (as reflected by the fact that none of the body pools had reached its isotopic steady state after 2 mo; Fig. 2). From these results, a practical adaptation of our versatile approach could consist in assessing FSR over periods shorter than the 2-mo period used in this study. As shown using noisy simulated data, restricting the experimental duration to 2 wk did not affect the accuracy of FSR estimates but impaired their precision, and more markedly for the slowly than for the rapidly turning-over tissues. This impaired precision may have resulted from numerical considerations, because fitting $\delta^{15}N$ postshift kinetics to sums of two exponential functions is more subject to error when the number of data points is decreased, particularly for tissues with a slow FSR, for which there is a greater uncertainty concerning the plateau values. Accordingly, when our approach is applied to the experimental data, the 2-mo and 2-wk FSR estimates differed more in muscle than in other tissues (Table 2), probably because the 2-wk FSR estimate was less accurate in such a slowly turning-over tissue, because of a greater impact of the experimental noise. To enable its application to shorter-term studies, it would be useful to adapt the experimental scheme to better characterize early postshift kinetics and reduce uncertainty in the fits. This could be achieved by increasing the number of sampling times and/or animals per sampling time over the shortened experimental duration. Finally, even if the truly informative time window is shorter if the FSR is high, longer-term values would remain useful on numerical grounds, since they do not deteriorate accuracy but ameliorate the precision of FSR estimations (by reducing the uncertainty of plateau $\delta^{15}N$ values). Consequently, whatever the FSR profile, it will always be useful to integrate long-term periods in the time window used for FSR estimation, whereas for a fast-FSR profile, omitting the truly informative, short-term period has a marked effect on the FSR estimation.

Cognitive Insights Into the P Metabolism of Tissues

We showed that although it is based on simplifying hypotheses, the representation of P turnover by a two-compartment model with a precursor-product structure is sufficient to account for the processes of P synthesis and breakdown in tissues such as liver, muscle, and kidney. By contrast, this precursor-product structure is too simple to adequately represent P turnover in skin and small intestine, which would require a model with more compartments and/or transfer pathways. Indeed, it is very likely that, in those tissues, the P or the AA compartment or both are not homogeneous and cannot be approximated by a single compartment. Consequently, a higher degree of compartmentation may be required for the AA pool, if the AA used as precursors for P synthesis and the AA derived from P breakdown do not mix, and/or for the P pool, if the tissue is composed of different P having distinct turnover rates.

In skin, the shape of the $\delta^{15}N$ kinetic curves was quite atypical, with $\delta^{15}N_P$ and $\delta^{15}N_{AA}$ kinetic curves that were less parallel than in other tissues, as $\delta^{15}N$ evolved particularly slowly in the P fraction. These kinetics could not be adequately fitted with our simple two-compartment model but were closely reproduced using a three-compartment structure that distinguished between two P compartments and included a flux of P disappearance from one of the compartments toward outside the system (Fig. 6). This more complex structure is actually consistent with the anatomy and physiology of skin, which is composed of two main layers, the dermis and the epidermis, which consist of different P (mostly collagen and keratin, respectively) with distinct turnover rates (55), and undergoes a direct loss of P by desquamation of the superficial epidermis. Interestingly, our results show that P turnover in skin involves a compartmentation of the P pool that probably results from its kinetic and spatial heterogeneity.

By contrast, concerning the small intestine, which we also identified as having a more compartmented P metabolism, the same three-compartment model accounting for P heterogeneity and desquamation did not enable a fit to its observed $\delta^{15}N$ kinetics. In this tissue, the compartmentation issue thus certainly also or rather involves the AA pool and, considering just one single and homogeneous AA compartment, probably constitutes an inadequate oversimplification. Indeed, the AA pool of the small intestine is probably highly heterogeneous, because AA arise from various sources (i.e., dietary and endogenous AA absorbed from the lumen, endogenous AA supplied via the artery, and AA derived from constitutive P breakdown) and are probably not uniformly mixed and indistinctly used for P synthesis. Extracellular AA (e.g., AA from plasma and/or the intestinal lumen) may be preferentially and directly supplied to P synthesis in this tissue through channeling without mixing with the intracellular pool (28, 52). As a result, the AA used for P synthesis and the AA derived from P breakdown would not completely mix and would have distinct $\delta^{15}N$ values. This specific compartmentation cannot be accounted for by a simple

model in which all AA are indiscriminately represented by one single AA compartment but would, instead, require a model that distinguishes two AA compartments, corresponding, respectively, to the AA precursors of P synthesis and those arising from P breakdown, as in some previously proposed theoretical representations (1, 35). Compartmentation of the AA pool is further supported by the differences in the isotopic enrichments of aminoacyl-tRNA (the true precursor for P synthesis) and intracellular AA in several tracer studies (1, 48, 52). In our study, the evolutions of the $\delta^{15}N$ were very similar in the sampled AA and P fractions of the small intestine (Fig. 2*E*), which is consistent with the hypothesis that the tissue free AA pool mainly represents AA arising from proteolysis in this tissue.

It should be noted that in plasma, where the P pool assembles P of different natures and origins, the precursors of protein synthesis are diverse (liver and, to a lesser extent, intestinal AA) and distinct from the products of proteolysis, since plasma P breakdown probably occurs in different tissues throughout the body (52). Consistent with this notion, we failed to estimate a plasma FSR value from our two-compartment model when using liver or intestinal data as $\delta^{15}N_{AA}$ values but succeeded when using plasma data. Although plasma AA were neither the true precursors nor the true products of plasma P synthesis and degradation, respectively, they were a valuable isotopic proxy for both, inasmuch as they provided a reasonable FSR estimate. This shows that it sometimes remains possible to find a way to estimate FSR by minimal modeling using a simple precursor-product structure, although the compartmentation is actually more complex.

Conclusions

We have demonstrated that the long-term evolutions of the $\delta^{15}N$ in the AA and P fractions of a tissue, following a change in the $\delta^{15}N$ of the diet, provide valuable cognitive and practical insights into its P metabolism. We evidenced that, for some tissues, such as liver, kidney, and muscle, a simple precursor-product model is well suited to describing the dynamics of P turnover, meaning that the AA and P pools are kinetically homogeneous enough to be each considered a single compartment. In these cases, we developed a numerical method that enables the determination of accurate and precise tissue FSR estimates from the $\delta^{15}N$ kinetics in the tissue P and AA fractions. Such FSR estimates represent integrated and averaged synthesis rates for all tissue P, on the condition that the time window is sufficiently broad to integrate rapidly and slowly turning-over P, and for all individual AA considered as a whole as precursors of P synthesis, over long periods of time and under real, nonartificially disturbed physiological conditions. On the basis of the $\delta^{15}N$ profiles, we also highlighted the fact that P turnover in skin and small intestine is too complex to be adequately described using a simple two-compartment model because of a higher degree of compartmentation in P and/or AA, which is consistent with the fact that the nutritional regulation of P turnover seems to be more atypical and complex in epithelia than in other tissues (4, 6, 54).

Perspectives and Significance

Our approach provides long-term FSR estimates that integrate the many diurnal variations in P kinetics that occur under sustained nutritional and physiological conditions; this feature is of particular interest to evaluating the global, integrated response of P turnover to a specific diet or treatment in nutrition and health. Furthermore, our approach provides new and important information regarding the structure and functioning of P turnover. Of the tissues sampled, only the intestine was identified as having a compartmentalized AA pool, probably because of the direct channeling of dietary and/or plasma AA for P synthesis. In the case of a substantial channeling of dietary AA, intestinal P synthesis would, to a great extent, be dependent on dietary AA input, which may explain why intestinal P synthesis is particularly sensitive to the route of nutrient supply, with parenteral (vs. enteral) nutrition leading to impaired protein synthesis and tissue atrophy (4). Interestingly, such a compartmentalized metabolism of precursor AA could be regarded as the organization that enables the intestine to fulfill the role imposed by its peculiar location: as the first organ to receive the nutrient influx, the intestine is expected to deal differentially with luminal and arterial AA, with specific utilization of dietary AA in the fed state to ensure maintenance of the intestinal P pool (because of its functional role in the absorptive capacity of the organism) and to moderate the postprandial rise in systemic AA concentrations (because the intestine ensures the homeodynamic control of nutrient transfer to plasma and tissues). Our approach may therefore constitute a promising tool to unravel the structural and functional characteristics of P metabolism in tissues.

APPENDIX

Here, we describe in detail the mathematical representation of the model presented in Fig. 1 and the derivation of the model equations *Eqs. 1* and *2*.

We used a simple two-compartment precursor-product structure, where the precursor compartment represents the free AA used for P synthesis and the product compartment represents the tissue P, to model AA and P metabolism in a given tissue. In this simple mathematical representation of the system, each of the two compartments is defined by two state variables: its total nitrogen content (N_{AA} and N_P, respectively) and its nitrogen isotopic enrichment ($\delta^{15}N_{AA}$ and $\delta^{15}N_P$, respectively).

The fluxes of total nitrogen ($N = {}^{14}N + {}^{15}N$) and heavy nitrogen isotope (^{15}N) between the model compartments were assumed to follow the mass action law and were modeled using the following equations

$$f_s(t) = k_s \times N_{AA}(t) \text{ and } {}^{15}f_s(t) = {}^{15}k_s \times {}^{15}N_{AA}(t)$$

$$f_d(t) = k_d \times N_P(t) \text{ and } {}^{15}f_d(t) = {}^{15}k_d \times {}^{15}N_P(t)$$

$$f_e(t) = k_e \times N_{AA}(t) \text{ and } {}^{15}f_e(t) = {}^{15}k_e \times {}^{15}N_{AA}(t)$$

where N_{AA} ($^{15}N_{AA}$) and N_P ($^{15}N_P$) represent the amount of total (heavy) nitrogen isotope in compartments AA and P, respectively, f_s ($^{15}f_s$), f_d ($^{15}f_d$), and f_e ($^{15}f_e$) represent the instantaneous fluxes of total (heavy) nitrogen transfer from AA to P through P synthesis, from P to AA through P breakdown, and from AA to the outside of the system through AA export toward the plasma, respectively, and k_s ($^{15}k_s$), k_d ($^{15}k_d$), and k_e ($^{15}k_e$) are the corresponding exchange rate constants for total (heavy) nitrogen. Because the biochemical processes involved in the metabolic reactions are sensitive to the isotope masses, the lighter nitrogen isotope (^{14}N) tends to react faster than the heavier nitrogen isotope (^{15}N), and isotope fractionation occurs during some metabolic reactions (30, 45, 46). To account for this potential isotope fraction-

ation, we assumed that the exchange rate constants would be different for total nitrogen and ^{15}N.

According to the mass conservation principle, the evolutions of total (heavy) nitrogen isotope in the AA and P compartments are described by the following equations

$$\frac{dN_P}{dt} = f_s - f_d, \quad \text{with} \frac{dN_P}{dt} = 0 \text{ by hypothesis, so that } f_s = f_d \tag{A1}$$

$$\frac{dN_{AA}}{dt} = f_0 - f_e + f_d - f_s, \quad \text{with} \frac{dN_{AA}}{dt} = 0 \text{ by hypothesis, so that } f_0 = f_e \tag{A2}$$

$$\frac{d^{15}N_{AA}(t)}{dt} = {}^{15}f_0(t) - {}^{15}f_e(t) + {}^{15}f_d(t) - {}^{15}f_s(t) \tag{A3}$$

$$\frac{d^{15}N_P(t)}{dt} = {}^{15}f_s(t) - {}^{15}f_d(t) \tag{A4}$$

where f_0 ($^{15}f_0$) represents the instantaneous flux of total (heavy) nitrogen transfer into AA from outside the system, i.e., from plasma. The simplifications in *Eqs. A1* and *A2* derived from the assumption that tissues have reached an elemental steady state at the time of the diet shift, i.e., that the amounts of total nitrogen in the compartments and the total nitrogen fluxes are constant.

By introducing the nitrogen fractional abundance F, defined as F = ^{15}N/N, the amounts of ^{15}N in the AA and P pools can be expressed as

$$^{15}N_{AA}(t) = N_{AA} \times F_{AA}(t)$$
$$^{15}N_P(t) = N_P \times F_P(t)$$

where F_{AA} and F_P are the fractional abundances in the AA and P pools, respectively.

Similarly, one can express the amounts of ^{15}N that are instantaneously exchanged between the model pools as

$$^{15}f_s(t) = f_s \times F_s(t)$$
$$^{15}f_d(t) = f_d \times F_d(t)$$
$$^{15}f_e(t) = f_e \times F_e(t)$$
$$^{15}f_0(t) = f_0 \times F_0(t)$$

where F_s, F_d, F_e, and F_0 are the fractional abundances in the corresponding instantaneous N fluxes f_s, f_d, f_e, and f_0.

Using the F notations and applying the Leibniz rule to calculate the derivatives of ($N_P \times F_P$) and ($N_A \times F_A$), we can rewrite *Eqs. A3* and *A4* as follows

$$N_{AA} \times \frac{d[F_{AA}(t)]}{dt} + F_{AA}(t) \times \frac{d(N_{AA})}{dt} = f_0 \times F_0(t) - f_e \times F_e(t) + f_d \times F_d(t) - f_s \times F_s(t) \tag{A5}$$

$$N_P \times \frac{d[F_P(t)]}{dt} + F_P(t) \times \frac{d(N_P)}{dt} = f_s \times F_s(t) - f_d \times F_d(t) \tag{A6}$$

which, under the steady-state assumptions for N_{AA} and N_P and combined with *Eqs. A1* and *A2*, simplify to

$$\frac{d[F_{AA}(t)]}{dt} = \frac{f_0}{N_{AA}} \times [F_0(t) - F_e(t)] + \frac{f_s}{N_{AA}} \times [F_d(t) - F_s(t)] \tag{A7}$$

$$\frac{d[F_P(t)]}{dt} = \frac{f_s}{N_P} \times [F_s(t) - F_d(t)] \tag{A8}$$

To express the model equations (*Eqs. A7* and *A8*) using the delta notations (δ^{15}N), we approximated the fractional abundance F (^{15}N/N) by the isotope ratio R (^{15}N/^{14}N) so that

$$F \approx R = R_{standard} \times \left(\frac{\delta}{1,000} + 1 \right)$$

where $R_{standard}$ is the nitrogen isotope ratio for the internationally defined standard (atmospheric N_2, $R_{standard}$ = 0.0036765).

Equations for the evolutions of the nitrogen isotopic enrichments in the AA ($\delta^{15}N_{AA}$) and P ($\delta^{15}N_P$) compartments can thus be derived from *Eqs. A7* and *A8* as follows

$$\frac{d[\delta^{15}N_{AA}(t)]}{dt} = \frac{f_0}{N_{AA}} \times [\delta^{15}N_0(t) - \delta^{15}N_e(t)] + \frac{f_s}{N_{AA}} \times [\delta^{15}N_d(t) - \delta^{15}N_s(t)] \tag{A9}$$

$$\frac{d[\delta^{15}N_P(t)]}{dt} = \frac{f_s}{N_P} \times [\delta^{15}N_s(t) - \delta^{15}N_d(t)] \tag{A10}$$

where $\delta^{15}N_s$, $\delta^{15}N_d$, $\delta^{15}N_e$, and $\delta^{15}N_0$ are the isotopic enrichments of the f_s, f_d, f_e, and f_0 instantaneous fluxes, respectively.

We defined ε_s, ε_d, and ε_e, the constant isotope effects associated with P synthesis, P breakdown, and AA export, as the difference between the isotopic enrichment of the instantaneous flux and that of its precursor pool, which yields the following equations

$$\varepsilon_s = \delta^{15}N_s(t) - \delta^{15}N_{AA}(t)$$
$$\varepsilon_d = \delta^{15}N_d(t) - \delta^{15}N_P(t)$$
$$\varepsilon_e = \delta^{15}N_e(t) - \delta^{15}N_P(t)$$

These relationships are usual approximations derived from the exact relationship $\varepsilon_{P/R} = (\alpha_{P/R} - 1) \times 1{,}000$, where the isotope fractionation factor $\alpha_{P/R}$ associated with a reaction linking R and P is defined as $\alpha_{P/R} = R_{Pi}/R_R \approx F_{Pi}/F_R = {}^{15}k_{P/R}/k_{P/R}$, where R_{Pi} and R_R are the isotope ratios in the instantaneous product (Pi) and reactant (R), respectively, and F_{Pi} and F_R are their fractional abundances (31).

We also defined the P FSR as the amount of P that is synthesized per day, relative to the size of the P pool

$$FSR = f_s/N_P$$

Using the ε and FSR notations, we can rewrite *Eqs. A9* and *A10* to yield the final equations describing the evolutions of the nitrogen isotopic enrichments in the AA and P compartments (see *Eqs. 1* and *2*, respectively)

$$\frac{d[\delta^{15}N_{AA}(t)]}{dt} = \frac{f_0}{N_{AA}} \times [\delta^{15}N_0(t) - \delta^{15}N_{AA}(t) - \varepsilon_e] + FSR \times \frac{N_P}{N_{AA}} \times [\delta^{15}N_P(t) - \delta^{15}N_{AA}(t) + \varepsilon_d - \varepsilon_s] \tag{A11}$$

$$\frac{d[\delta^{15}N_P(t)]}{dt} = FSR \times [\delta^{15}N_{AA}(t) - \delta^{15}N_P(t) + \varepsilon_s - \varepsilon_d] \tag{A12}$$

At isotopic equilibrium, i.e., when $d[\delta^{15}N_P(t)]/dt = 0$, then $\Delta\varepsilon = \varepsilon_s - \varepsilon_d = \delta^{15}N_P - \delta^{15}N_{AA}$.

By integrating *Eq. A12*, the change in δ^{15}N in the P compartment over a time interval Δt can be expressed as

$$\delta^{15}N_P(t) = FSR \times \left[\int_t^{t+\Delta t} \delta^{15}N_A(t) \cdot dt - \int_t^{t+\Delta t} \delta^{15}N_P(t) \cdot dt \right] + FSR \times \Delta\varepsilon \times \Delta t \tag{A13}$$

where $\Delta\delta^{15}N_P(t) = \delta^{15}N_P(t + \Delta t) - \delta^{15}N_P(t)$ and $\Delta\varepsilon = (\varepsilon_s - \varepsilon_d)$.

When N_{AA} and N_P are not assumed to be in steady state, *Eq. A13* is modified as follows

$$\Delta\delta^{15}N_P(t) = FSR \times \left[\int_t^{t+\Delta t} \delta^{15}N_A(t)\cdot dt - \int_t^{t+\Delta t} \delta^{15}N_P(t)\cdot dt\right] + FSR \times \Delta\varepsilon \times \Delta t + FGR \times \varepsilon_d \times \Delta t \quad (A14)$$

where FGR is the fractional growth rate of the P compartment, defined as $FGR = 1/N_P \times dN_P/dt$.

ACKNOWLEDGMENTS

We thank Dr. M. Sebilo and his research team BIOEMCO (UMR 7618, Université Pierre et Marie Curie, Paris, France) for supplying the internal standard for isotopic measurements and the three anonymous reviewers for useful comments on the earlier version of the manuscript.

DISCLOSURES

No conflicts of interest, financial or otherwise, are declared by the authors.

AUTHOR CONTRIBUTIONS

N.P. and H.F. are responsible for conception and design of the research; N.P., J.-F.H., F.M., C.B., and H.F. performed the experiments; N.P. and H.F. analyzed the data; N.P., J.-F.H., F.M., and H.F. interpreted the results of the experiments; N.P. prepared the figures; N.P. and H.F. drafted the manuscript; N.P., J.-F.H., F.M., D.T., and H.F. edited and revised the manuscript; N.P., J.-F.H., F.M., D.T., and H.F. approved the final version of the manuscript.

REFERENCES

1. **Airhart J, Vidrich A, Khairallah EA.** Compartmentation of free amino acids for protein synthesis in rat liver. *Biochem J* 140: 539–545, 1974.
2. **Baillie AG, Garlick PJ.** Attenuated responses of muscle protein synthesis to fasting and insulin in adult female rats. *Am J Physiol Endocrinol Metab* 262: E1–E5, 1992.
3. **Baillie AG, Garlick PJ.** Protein synthesis in adult skeletal muscle after tenotomy: responses to fasting and insulin infusion. *J Appl Physiol* 71: 1020–1024, 1991.
4. **Baracos VE, Samuels SE, Adegoke OA.** Anabolic and catabolic mediators of intestinal protein turnover: a new experimental approach. *Curr Opin Clin Nutr Metab Care* 3: 183–189, 2000.
5. **Bijsterbosch MK, Duursma AM, Bouma JMW, Gruber M.** The plasma-volume of the Wistar rat in relation to the body-weight. *Experientia* 37: 381–382, 1981.
6. **Biolo G, Gastaldelli A, Zhang XJ, Wolfe RR.** Protein synthesis and breakdown in skin and muscle: a leg model of amino acid kinetics. *Am J Physiol Endocrinol Metab* 267: E467–E474, 1994.
7. **Boutry C, Fouillet H, Mariotti F, Blachier F, Tome D, Bos C.** Rapeseed and milk protein exhibit a similar overall nutritional value but marked difference in postprandial regional nitrogen utilization in rats. *Nutr Metab* 8: 52, 2011.
8. **Cherel Y, Attaix D, Rosolowska-Huszcz D, Belkhou R, Robin JP, Arnal M, Le Maho Y.** Whole-body and tissue protein synthesis during brief and prolonged fasting in the rat. *Clin Sci (Lond)* 81: 611–619, 1991.
9. **Chevalier L, Bos C, Azzout-Marniche D, Dardevet D, Tome D, Gaudichon C.** Dietary protein regulates hepatic constitutive protein anabolism in rats in a dose-dependent manner and independently of energy nutrient composition. *Am J Physiol Regul Integr Comp Physiol* 299: R1720–R1730, 2010.
10. **Chevalier L, Bos C, Gryson C, Luengo C, Walrand S, Tome D, Boirie Y, Gaudichon C.** High-protein diets differentially modulate protein content and protein synthesis in visceral and peripheral tissues in rats. *Nutrition* 25: 932–939, 2009.
11. **Danicke S, Nieto R, Lobley GE, Fuller MF, Brown DS, Milne E, Calder AG, Chen S, Grant I, Bottcher W.** Responses in the absorptive phase in muscle and liver protein synthesis rates of growing rats. *Arch Tierernahr* 52: 41–52, 1999.
12. **Davis TA, Reeds PJ.** Of flux and flooding: the advantages and problems of different isotopic methods for quantifying protein turnover in vivo. II. Methods based on the incorporation of a tracer. *Curr Opin Clin Nutr Metab Care* 4: 51–56, 2001.
13. **El Yousfi M, Breuille D, Papet I, Blum S, Andre M, Mosoni L, Denis P, Buffiere C, Obled C.** Increased tissue protein synthesis during spontaneous inflammatory bowel disease in HLA-B27 rats. *Clin Sci (Lond)* 105: 437–446, 2003.
14. **Estornell E, Barber T, Cabo J.** Protein synthesis in vivo in rats fed on lipid-rich liquid diets. *Br J Nutr* 72: 509–517, 1994.
15. **Estornell E, Cabo J, Barber T.** Protein synthesis is stimulated in nutritionally obese rats. *J Nutr* 125: 1309–1315, 1995.
16. **Faure M, Chone F, Mettraux C, Godin JP, Bechereau F, Vuichoud J, Papet I, Breuille D, Obled C.** Threonine utilization for synthesis of acute phase proteins, intestinal proteins, and mucins is increased during sepsis in rats. *J Nutr* 137: 1802–1807, 2007.
17. **Faure M, Moennoz D, Montigon F, Fay LB, Breuille D, Finot PA, Ballevre O, Boza J.** Development of a rapid and convenient method to purify mucins and determine their in vivo synthesis rate in rats. *Anal Biochem* 307: 244–251, 2002.
18. **Faure M, Moënnoz D, Montigon F, Mettraux C, Breuillé D, Ballèvre O.** Dietary threonine restriction specifically reduces intestinal mucin synthesis in rats. *J Nutr* 135: 486–491, 2005.
19. **Fouillet H, Bos C, Gaudichon C, Tome D.** Approaches to quantifying protein metabolism in response to nutrient ingestion. *J Nutr* 132: 3208S–3218S, 2002.
20. **Garlick PJ, McNurlan MA, Essen P, Wernerman J.** Measurement of tissue protein synthesis rates in vivo: a critical analysis of contrasting methods. *Am J Physiol Endocrinol Metab* 266: E287–E297, 1994.
21. **Gasier HG, Riechman SE, Wiggs MP, Previs SF, Fluckey JD.** A comparison of ^2H_2O and phenylalanine flooding dose to investigate muscle protein synthesis with acute exercise in rats. *Am J Physiol Endocrinol Metab* 297: E252–E259, 2009.
22. **Gaudichon C, Bos C, Morens C, Petzke KJ, Mariotti F, Everwand J, Benamouzig R, Dare S, Tome D, Metges CC.** Ileal losses of nitrogen and amino acids in humans and their importance to the assessment of amino acid requirements. *Gastroenterology* 123: 50–59, 2002.
23. **Goldspink DF, Kelly FJ.** Protein turnover and growth in the whole body, liver and kidney of the rat from the foetus to senility. *Biochem J* 217: 507–516, 1984.
24. **Jeejeebhoy KN, Bruce-Robertson A, Ho J, Sodtke U.** The effect of cortisol on the synthesis of rat plasma albumin, fibrinogen and transferrin. *Biochem J* 130: 533–538, 1972.
25. **Jepson MM, Bates PC, Millward DJ.** The role of insulin and thyroid hormones in the regulation of muscle growth and protein turnover in response to dietary protein in the rat. *Br J Nutr* 59: 397–415, 1988.
26. **Johnson HA, Baldwin RL, France J, Calvert CC.** A model of whole-body protein turnover based on leucine kinetics in rodents. *J Nutr* 129: 728–739, 1999.
27. **Johnson HA, Baldwin RL, France J, Calvert CC.** Recycling, channeling and heterogeneous protein turnover estimation using a model of whole-body protein turnover based on leucine kinetics in rodents. *J Nutr* 129: 740–750, 1999.
28. **Johnson HA, Baldwin RL, Klasing KC, Calvert CC.** Impact of separating amino acids between plasma, extracellular and intracellular compartments on estimating protein synthesis in rodents. *Amino Acids* 20: 389–400, 2001.
29. **Laurent BC, Moldawer LL, Young VR, Bistrian BR, Blackburn GL.** Whole-body leucine and muscle protein kinetics in rats fed varying protein intakes. *Am J Physiol Endocrinol Metab* 246: E444–E451, 1984.
30. **Macko SA, Estep MLF, Engel MH, Hare PE.** Kinetic fractionation of stable nitrogen isotopes during amino-acid transamination. *Geochim Cosmochim Acta* 50: 2143–2146, 1986.
31. **Mariotti A, Mariotti F, Champigny ML, Amarger N, Moyse A.** Nitrogen isotope fractionation associated with nitrate reductase activity and uptake of NO_3^- by pearl-millet. *Plant Physiol* 69: 880–884, 1982.
32. **Masanes RM, Fernandez-Lopez JA, Alemany M, Remesar X, Rafecas I.** Effect of dietary protein content on tissue protein synthesis rates in Zucker lean rats. *Nutr Res* 19: 1017–1010, 1999.
33. **McNurlan MA, Fern EB, Garlick PJ.** Failure of leucine to stimulate protein synthesis in vivo. *Biochem J* 204: 831–838, 1982.
34. **Mercier S, Breuille D, Mosoni L, Obled C, Patureau Mirand P.** Chronic inflammation alters protein metabolism in several organs of adult rats. *J Nutr* 132: 1921–1928, 2002.
35. **Mortimore GE, Woodside KH, Henry JE.** Compartmentation of free valine and its relation to protein turnover in perfused rat liver. *J Biol Chem* 247: 2776–2784, 1972.
36. **Mosoni L, Valluy MC, Serrurier B, Prugnaud J, Obled C, Guezennec CY, Mirand PP.** Altered response of protein synthesis to nutritional state and endurance training in old rats. *Am J Physiol Endocrinol Metab* 268: E328–E335, 1995.
37. **Papet I, Dardevet D, Sornet C, Bechereau F, Prugnaud J, Pouyet C, Obled C.** Acute phase protein levels and thymus, spleen and plasma protein synthesis rates differ in adult and old rats. *J Nutr* 133: 215–219, 2003.

38. **Poupin N, Bos C, Mariotti F, Huneau JF, Tome D, Fouillet H.** The nature of the dietary protein impacts the tissue-to-diet N discrimination factors in laboratory rats. *PLos One* 6: e28046, 2011.
39. **Preedy VR, Garlick PJ.** Protein synthesis in skeletal muscle of the perfused rat hemicorpus compared with rates in the intact animal. *Biochem J* 214: 433–442, 1983.
40. **Preedy VR, McNurlan MA, Garlick PJ.** Protein synthesis in skin and bone of the young rat. *Br J Nutr* 49: 517–523, 1983.
41. **Reeds PJ, Davis TA.** Of flux and flooding: the advantages and problems of different isotopic methods for quantifying protein turnover in vivo. I. Methods based on the dilution of a tracer. *Curr Opin Clin Nutr Metab Care* 2: 23–28, 1999.
42. **Ruot B, Bechereau F, Bayle G, Breuille D, Obled C.** The response of liver albumin synthesis to infection in rats varies with the phase of the inflammatory process. *Clin Sci (Lond)* 102: 107–114, 2002.
43. **Ruot B, Breuille D, Rambourdin F, Bayle G, Capitan P, Obled C.** Synthesis rate of plasma albumin is a good indicator of liver albumin synthesis in sepsis. *Am J Physiol Endocrinol Metab* 279: E244–E251, 2000.
44. **Samuels SE, Taillandier D, Aurousseau E, Cherel Y, Le Maho Y, Arnal M, Attaix D.** Gastrointestinal tract protein synthesis and mRNA levels for proteolytic systems in adult fasted rats. *Am J Physiol Endocrinol Metab* 271: E232–E238, 1996.
45. **Seila AC, Okuda K, Nunez S, Seila AF, Strobel SA.** Kinetic isotope effect analysis of the ribosomal peptidyl transferase reaction. *Biochemistry* 44: 4018–4027, 2005.
46. **Silfer JA, Engel MH, Macko SA.** Kinetic fractionation of stable carbon and nitrogen isotopes during peptide-bond hydrolysis—experimental-evidence and geochemical implications. *Chem Geol* 101: 211–221, 1992.
47. **Slevin K, Waterlow J.** Theoretical analysis of the importance of recycling in measurements of protein turnover by constant infusion of a labelled amino acid. *J Theor Biol* 253: 215–219, 2008.
48. **Smith CB, Sun Y.** Influence of valine flooding on channeling of valine into tissue pools and on protein synthesis. *Am J Physiol Endocrinol Metab* 268: E735–E744, 1995.
49. **Smith GI, Villareal DT, Mittendorfer B.** Measurement of human mixed muscle protein fractional synthesis rate depends on the choice of amino acid tracer. *Am J Physiol Endocrinol Metab* 293: E666–E671, 2007.
50. **Taillandier D, Guezennec CY, Patureau-Mirand P, Bigard X, Arnal M, Attaix D.** A high protein diet does not improve protein synthesis in the non-weight-bearing rat tibialis anterior muscle. *J Nutr* 126: 266–272, 1996.
51. **Toffolo G, Foster DM, Cobelli C.** Estimation of protein fractional synthetic rate from tracer data. *Am J Physiol Endocrinol Metab* 264: E128–E135, 1993.
52. **Waterlow JC.** *Protein Turnover*. Wallingford, UK: CABI, 2006, p. 301.
53. **Wolfe RR, Chinkes DL.** *Isotope Tracers in Metabolic Research: Principles and Practice of Kinetic Analysis*. New York: Wiley-Liss, 2005, p. 474.
54. **Zhang XJ, Chinkes DL, Doyle D Jr, Wolfe RR.** Metabolism of skin and muscle protein is regulated differently in response to nutrition. *Am J Physiol Endocrinol Metab* 274: E484–E492, 1998.
55. **Zhang XJ, Chinkes DL, Wolfe RR.** Measurement of protein metabolism in epidermis and dermis. *Am J Physiol Endocrinol Metab* 284: E1191–E1201, 2003.